 doi:10.20944/preprints202103.0615.v1

Article

A POSSIBLE RESOLUTION TO TROUBLES OF SU(2) CENTER VORTEX DETECTION IN SMOOTH LATTICE CONFIGURATIONS

Rudolf Golubich *, Manfried Faber

Atominstitut, Technische Universität Wien; 1040 Wien; Austria
* rudolf.golubich@gmail.com

Abstract: The *center vortex model* of quantum-chromodynamics can explain confinement and chiral symmetry breaking. We present a possible resolution for problems of the vortex detection in smooth configurations and discuss improvements for the detection of center vortices.

Keywords: quantum chromodynamics; confinement; center vortex model; vacuum structure; cooling

PACS: 11.15.Ha, 12.38.Gc

1. Introduction

The center vortex model of Quantum Chromodynamics [1,2] explains confinement [3] and chiral symmetry breaking [4–6] by the assumption that the relevant excitations of the QCD vacuum are Center vortices: Closed color magnetic flux lines evolving in time. In four dimensional space-time these closed flux lines form closed surfaces in dual space, see Figure 1. In the low temperature phase they percolate space-time in all dimensions. Within lattice simulations the center vortices are detected in *maximal center*

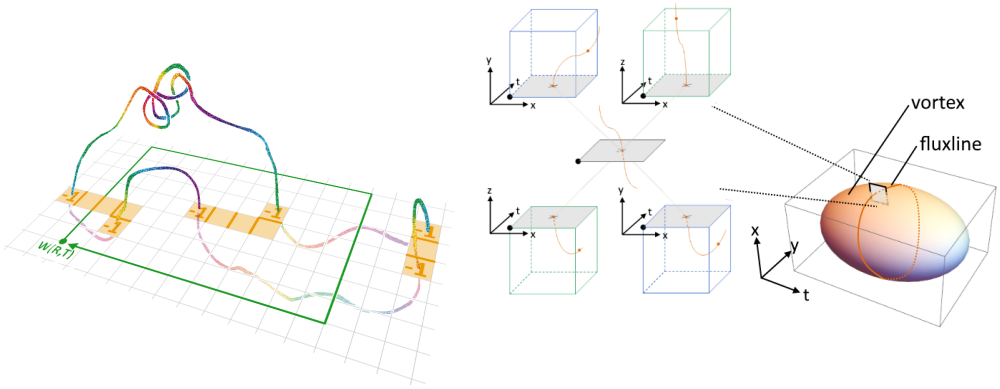

Figure 1. left) After transformation to maximal center gauge and projection to the center degrees of freedom, a flux line can be traced by following non-trivial plaquettes. right) Due to the evolution in time such a flux can be traced in two dimensions. In dual space this results in a closed vortex surface.

gauge after projection to the center degrees of freedom. The procedure is described in more detail in section 2. As long as the detected vortices reproduce the relevant physics we speak of a valid *vortex finding property*. During the analysis of the color structure of vortices in smooth configurations [7] one is confronted with a loss of the vortex finding property. Problems at detecting center vortices due to ambiguities at the gauge fixing

Preprints (www.preprints.org) | NOT PEER-REVIEWED | Posted: 25 March 2021 doi:10.20944/preprints202103.0615.v1

procedure have already been found by Kovacs and Tomboulis [8]. They also point out that *thick vortices* are of importance when calculating the path integral. We found, that the thickness of vortices can cause troubles for the vortex detection, resulting in a loss of the string tension. In search for improvements of the vortex detection the cause of this loss is analyzed and a possible resolution discussed. An upper limit for the lattice spacing and a lower limit for the lattice size is presented. These limits are derived from measurements of the vortex density and estimates of the cross-section of flux tubes.

2. Materials and Methods

The lattice simulation in use is based on gluonic SU(2) Wilson action with inverse coupling β covering an interval from $\beta = 2.1$ to $\beta = 3.6$ in steps of 0.05. The corresponding lattice spacing a is determined by assuming a physical string tension of $(440\ \mathrm{MeV})^2$ via a cubic interpolation of literature values given in Table 1 and complemented by an extrapolation according to the asymptotic renormalization group equation

$$a(\beta) = \Lambda^{-1} e^{-\frac{\beta}{8\beta_0}} \quad \text{with} \quad \beta_0 = \frac{11}{24\pi^2} \quad \text{and} \quad \Lambda = 0.015(2)\mathrm{fm}^{-1}. \tag{1}$$

β	2.3	2.4	2.5	2.635	2.74	2.85
a [fm]	0.165(1)	0.1191(9)	0.0837(4)	0.05409(4)	0.04078(9)	0.0296(3)
σ [lattice]	0.136(2)	0.071(1)	0.0350(4)	0.01459(2)	0.00830(4)	0.00438(8)

Table 1: The values of the lattice spacing in fm and the string tension corresponding to the respective value of β are taken from Refs. [9–13], setting the physical string tension to $(440\ \mathrm{MeV})^2$.

The analysis is performed on lattices of size 8^4 and 10^4 with 0, 1, 2, 3, 5 and 10 Pisa-Cooling [14] steps with a cooling parameter of 0.05. A central part consists in identifying non-tivial center regions using the algoithms presented in Refs. [15–17]. In the gauge fixing procedure we look for gauge matrices Ω that maximize the functional

$$R^2 = \sum_x \sum_\mu |\ \mathrm{Tr}[\acute{U}_\mu(x)]\ |^2 \quad \text{with} \quad \acute{U}_\mu(x) = \Omega(x + e_\mu) U_\mu(x) \Omega^\dagger(x). \tag{2}$$

Non-trivial center regions are used to guide this procedure to prevent the problems found by Bornyakov et al. in [18] as is explained in detail in the listed references. After the gauge is fixed, those plaquettes are identified that evaluate to the non-trivial center element after projection of the configuration to the center degrees of freedom. These plaquettes are considered pierced by a P-vortex.

If the count of P-plaquettes is below the count of non-trivial center regions used to guide the gauge fixing procedure, it is a clear indication of a failing vortex detection. For each value of β the proportion of configurations where this is the case is determined. This allows to quantify the loss of the vortex finding property besides quantifying it directly via the string tension of the center projected configurations.

The further analysis is performed in the full SU(2) configurations. For each P-plaquette a non-trivial center region that encloses the P-plaquette is identified. This center region is considered to be pierced by the thick vortex that is detected by the P-vortex. Figure 2 depicts the relation between P-vortices and thick vortices.

The cross-section of the flux building the thick thick vortex, A_{vort}, is measured by counting the plaquettes that build up the non-trivial center regions enclosing the corresponding thick vortex. In each configuration we determine minimal, average and maximal cross-sections.

Preprints (www.preprints.org) | NOT PEER-REVIEWED | Posted: 25 March 2021 doi:10.20944/preprints202103.0615.v1

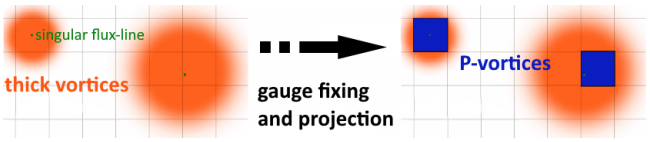

Figure 2. Vortex detection as a best fit procedure of P-Vortices to thick vortices shown in a two dimensional slice through a four dimensional lattice.

The string tension σ is determined via Creutz ratios χ calculated in the center projected configurations

$$\sigma \approx \chi(R,T) = -\ln \frac{\langle W(R+1,T+1)\rangle \, \langle W(R,T)\rangle}{\langle W(R,T+1)\rangle \, \langle W(R+1,T)\rangle}, \tag{3}$$

with $R \times T$ Wilson loops $W(R,T)$. As the Coloumb-part of the potential is strongly suppressed after projecting to the center degrees of freedom, the linear part corresponding to a non-vanishing string tension is already reproduced with small loop sizes. Symmetric Creutz ratios are used and the average of $\chi(1,1)$ and $\chi(2,2)$ is taken to determine the string tension. Assuming independence of vortex piercings, the string tension can also be related to the vortex density ϱ_{vort}, the number of P-plaquettes per unit volume, via

$$\sigma \approx -\ln(1 - 2 * \varrho_{\mathrm{vort}}). \tag{4}$$

The requirement of uncorrelated piercing is only fulfilled if the vortex surface is strongly smoothed, otherwise this simple equation overestimates the string tension.

The working hypothesis is that the loss of the vortex finding property, observed via a loss of the string tension, when cooling is applied, can be related to a thickening of the vortices.

3. Results

The different measurements are performed for a lot of different values of β and several cooling steps. As not to overload the visualizations only a part of the intermediate results is depicted, showing only specific numbers of cooling steps and restricting to a smaller interval of β-values. Those parts of the data that are dominated by finite size effects are identified and excluded from the further analysis.

Starting with the quantification of the vortex finding property presented in Figure 3 some troubles are brought to light. The proportion of configurations where less P-plaquettes have been identified than non-trivial center regions exist, rises rapidly when passing a specific value of β. This specific value depends on the lattice size and the number of cooling steps. . When reducing the lattice size or increasing the number of cooling steps the loss of the vortex finding property occurs at lowered values of β. The proportion depicted seems to saturate at about 30%, except for 10 cooling steps at a lattice of size 8^4 where it reaches higher values. The fact that some non-trivial center regions have no corresponding P-plaquettes after gauge fixing and projection to the center degrees of freedom hints at a possible explanation for part of the lost string tension: The gauge functional given in Equation (2) is local in the sense that each gauge matrix Ω is solely based on the 8 gluonic links connected to the specific lattice point. Farther distances than a single lattice spacing are not taken into account directly. In contrast, the detection of the non-trivial center regions is in a sense more physical as it is based solely on gauge independent quantities, that is, the evaluation of arbitrary big Wilson loops. When detecting P-vortices in smooth configurations and high lattice resolutions, the center flux can be distributed over many link variables. Each of these links can evaluate arbitrarily close to the trivial center element although a Wilson loop build by the links can evaluate arbitrarily near to the non-trivial center element. In such

Preprints (www.preprints.org) | NOT PEER-REVIEWED | Posted: 25 March 2021 doi:10.20944/preprints202103.0615.v1

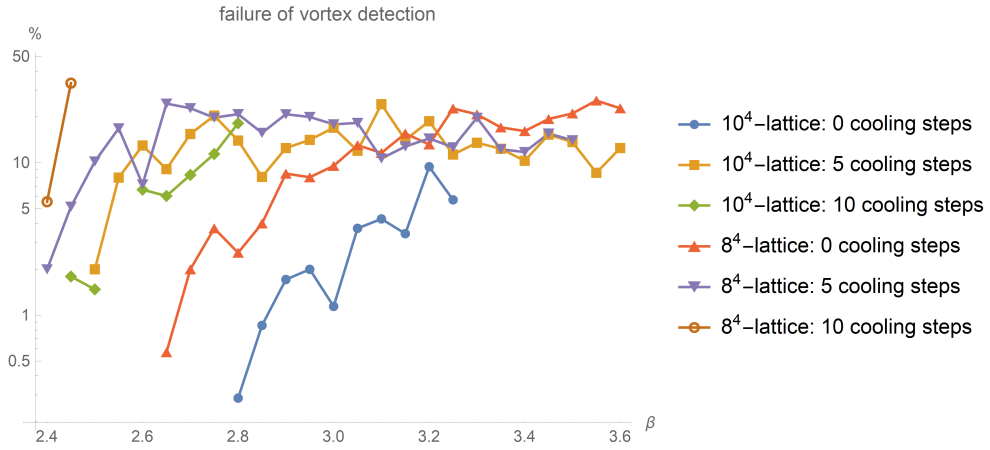

Figure 3. The proportion of configurations is depicted where less non-trivial plaquettes have been identified than non-trivial regions exist. The datapoints are joined to guide the eye. Due to the logarithmic scaling of axes only non-vanishing values are depicted. Observe that the curves rise at different values of β for different number of cooling steps and different lattice sizes.

a scenario a gauge fixing procedure, only taking the vicinity of lattice points into account, will likely fail and result in an underestimated string tension.

Looking at the Creutz ratios depicted in Figure 4 two possibly intertwined effects can be observed. At sufficiently low values of β the string tension is independent of the

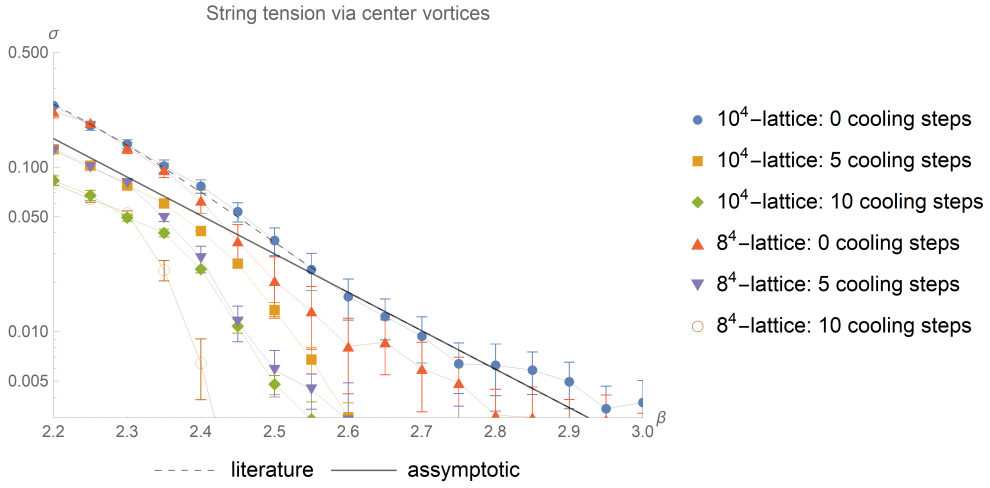

Figure 4. The string tension σ is estimated via an average of the Creutz ratios $\chi(1,1)$ and $\chi(2,2)$ calculated in center projected configurations for different numbers of cooling steps and lattice sizes. The datapoints are joined by lines to guide the eye. The literature values correspond to those listed in Table 1, the asymptotic line is given by Equation (1). Observe that in the low β-regime an underestimation of the string tension correlates to the number of cooling steps. This underestimation is independent of the lattice size. At higher values of β finite size effects set in.

lattice size, but decreases with an increasing number of cooling steps. Of interest is that for sufficiently small values of β the deviation from the asymptotic prediction decreases with a rising value of β. At higher values of β the independence from the lattice size no longer holds. For different lattice sizes a sudden decrease of the string tension occurs at different values of β. The respective β-values are compatible for different numbers of cooling steps. The dependency on the lattice size and the independence on the number of cooling steps hint at finite size effects, but finite size effects do not give a direct explanation of the reduction of the string tension at lower values of β: We do not observe

Preprints (www.preprints.org) | NOT PEER-REVIEWED | Posted: 25 March 2021 doi:10.20944/preprints202103.0615.v1

a dependency on the lattice size in the low β-regime. Based on the deviations of the string tensions for different lattice sizes we expect finite size effects to occur at length scales between 1.1 fm and 1.3 fm, independent of cooling. This length scales are above 1 fm as was already hinted at by Kovacs and Tomboulis [19]. In Ref. [7] we found also color-homogeneous regions with extensions compatible with these values. A compatible distance can also be found between neighbouring piercings of a Wilson loop, extracted from the vortex density.

A relation to the thickness A_{vort} of center vortices is suspected and points towards possible further analysis. The possibility of a thick vortex to expand due to a spreading of the center flux was already suggested by Kovacs and Tomboulis in [20]. Assuming a circular cross-section of the flux tube, its diameter can be calculated as

$$d_{\text{flux}} = 2 * \underbrace{\sqrt{\frac{A_{\text{vort}}}{\pi}}}_{r_{\text{flux}}}, \tag{5}$$

with A_{vort} being the area of the flux cross-section. That flux lines are closed requires that within each two dimensional slice through the lattice at least two vortex piercings can find place. This give a criteria on the lattice extent L:

$$L > 2 * d_{\text{flux}}. \tag{6}$$

If A_{vort} measured by a plaquette count exceeds 19 for a lattice of size 10^4, or 12 for a lattice of size 8^4, we can expect finite size effects to step in. These thresholds are of relevance for the average, minimal and maximal flux tube cross-section depicted in Figures 5, 6 and 7. The mean flux tube cross-section presented in Figure 5 shows that we have to restrict to relative low values of β to stay away from finite size effects. Taking a

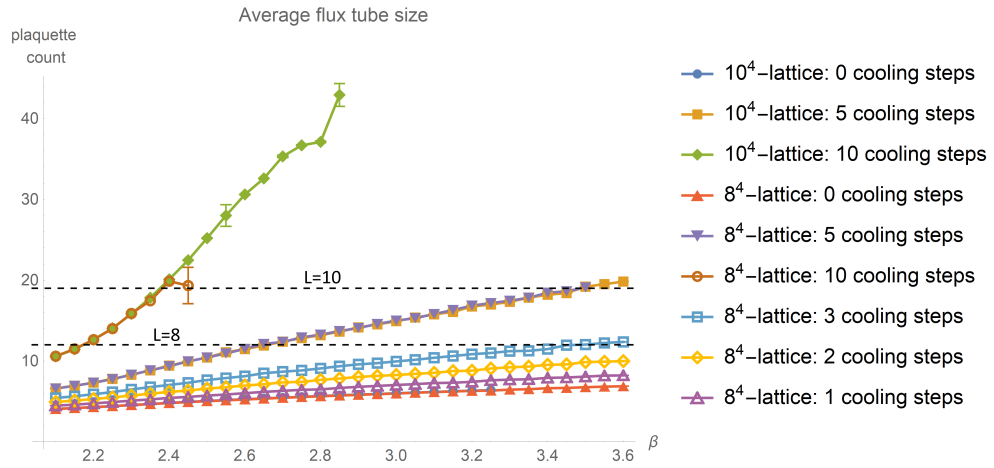

Figure 5. The average cross-sections of the flux tubes, measured by counting plaquettes, increases when cooling is applied. It reaches a threshold at which finite size effects are expected to become problematic, shown as dashed line for the two lattice sizes. Measurements performed on lattices of different size are in good compatibility.

look at the maximal flux tube cross-section depicted in Figure 6, we can expect finite size effects at even lower values of β: None of the data with 10 cooling steps can be expected to be free of finite size effects. The lattice of size 8^4 could be too small even without any cooling applied. With an increased number of cooling steps the compatibility of different lattice sizes gets reduced but it is still given for sufficiently low numbers of cooling steps.

Taking a look at the minimal tube size depicted in Figure 7 an even more sudden rise of the cross-section can be observed. We expect that the minimal flux tube cross-sections starts to grow with a certain β, where the high action density of non-trivial plaquettes

Preprints (www.preprints.org) | NOT PEER-REVIEWED | Posted: 25 March 2021 doi:10.20944/preprints202103.0615.v1

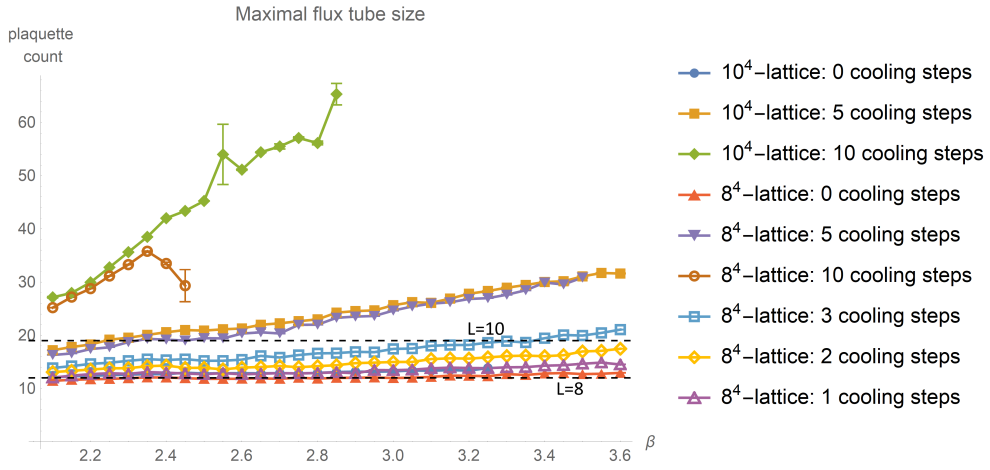

Figure 6. The maximal cross-sections of the flux tubes hint at finite size effects. Within our β-interval only the lattice of size 10^4 stays below the threshold when cooling is applied. The compatibility of different lattice sizes is only given for sufficiently low numbers of cooling steps.

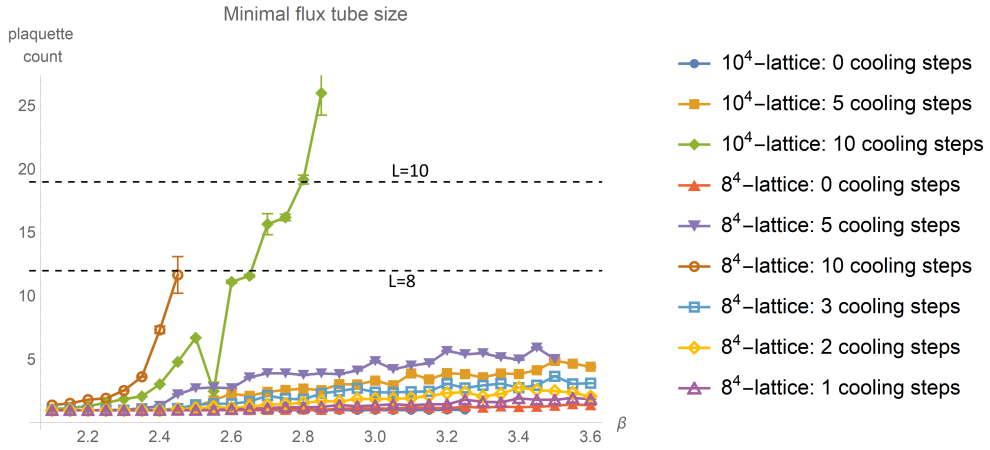

Figure 7. The minimal size of the flux tubes cross-sections shows a strong dependency on the lattice size. This dependency becomes even stronger when cooling is applied. Only with at most 3 cooling steps applied, the data seem thrust-worthy for $\beta < 2.3$.

leads to a suppression in the path integral. This causes a dependency on the lattice size due to the reduced statistics. For sufficiently low values of β and sufficiently low numbers of cooling steps the minimal flux tube cross-section is given by exactly one plaquette, independent of β and the number of cooling steps. We restrict the further analysis to the lattice of size 10^4 with $\beta \leq 2.3$ and at most 5 cooling steps. This concludes the identification of those parts of the data, that are flawed by finite size effects or a lack of statistics.

Assuming an exponential growth of the flux tubes cross section with an increase in the number of cooling steps a model of the form

$$A_{\text{vort}}(N_{\text{cool}}) = A_{\text{vort}}(0)\, e^{N_{\text{cool}}\,(g_{\text{cool}} + g_{\text{discret}}\,a)} \tag{7}$$

is fit to the data with N_{cool} being the number of cooling steps and a the lattice spacing. The fit-parameter g_{cool} corresponds to the exponential growth of the flux tube with cooling. As the tube size is measured by counting plaquettes we have to account for discretization effects. This is done by adding another fit-parameter g_{discret} in the exponent that is related to the lattice constant and the number of cooling steps. The two

Preprints (www.preprints.org) | NOT PEER-REVIEWED | Posted: 25 March 2021 doi:10.20944/preprints202103.0615.v1

parameters are not necessarily constant as they can depend on the specific structure of interest. We restrain from carrying along another index: In the following the values of these two parameters are to be considered only with respect to the specific given context. They differ for the average cross-sections and the maximal cross-sections of flux tubes. The fit of this model to the average flux tube sizes is shown in Figure 8 in physical units. The fit is done for small β and cooling steps indicated by black points. The fit, dashed

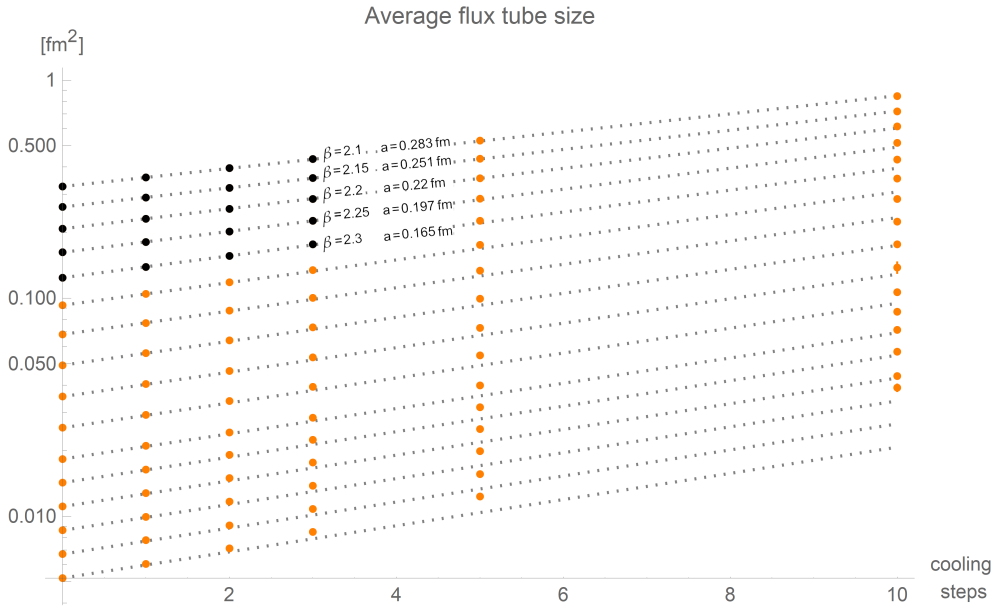

Figure 8. The measured data of the average flux tube cross-section for various numbers of cooling steps and several β are shown by black and orange points. The dashed lines depict the fits according to Equation (7), where only the black data points were used. The corresponding fit parameters are given in Table 2. Deviations of the data from the fits can be related to finite size effects.

lines, reproduce the data well until the expected onset of finite size effects for cross-sections increasing with the number of cooling steps and β. This onset is compatible to the estimates in Equation (6) and will be discussed later. Now we concentrate on the growing of the flux tube cross-section described by the fit parameters given in Table 2. The suspected exponential growth of A_{vort} is confirmed by the good quality of the fit for positive g_{cool} even for larger values of β and cooling steps. The negative value

average cross-sections	Estimate	t-Statistic	P-Value
g_{cool}	0.14(1)	13.6393	$6.3 * 10^{-11}$
g_{discret}	-0.17(5) fm^{-1}	-3.62376	$1.9 * 10^{-3}$

Table 2: Shown are the parameters of the model described by Equation (7) and depicted in Figure 9 for average cross-sections.

of g_{discret} reflects the decreasing slope of the dashed lines with increasing β, indicating an influence of the lattice resolution: A coarser lattice reduces the growth of A_{vort}. The overall behaviour of A_{vort} is qualitatively reproduced by the maximal cross-sections as is depicted in Figure 9. Only the growth has slowed down as can be seen at the values given in Table 3. This implies that the growth of A_{vort} with increased cooling is limited.

A further influence of cooling is a smoothing of the vortex surface. We will now model this smoothing and show that the vortex flux tubes can be thickened without pushing each other apart. The vortex density ϱ_{vort} allows to gain information about the distance of the vortex centers. Here we have to take into account that some of

Preprints (www.preprints.org) | NOT PEER-REVIEWED | Posted: 25 March 2021 doi:10.20944/preprints202103.0615.v1

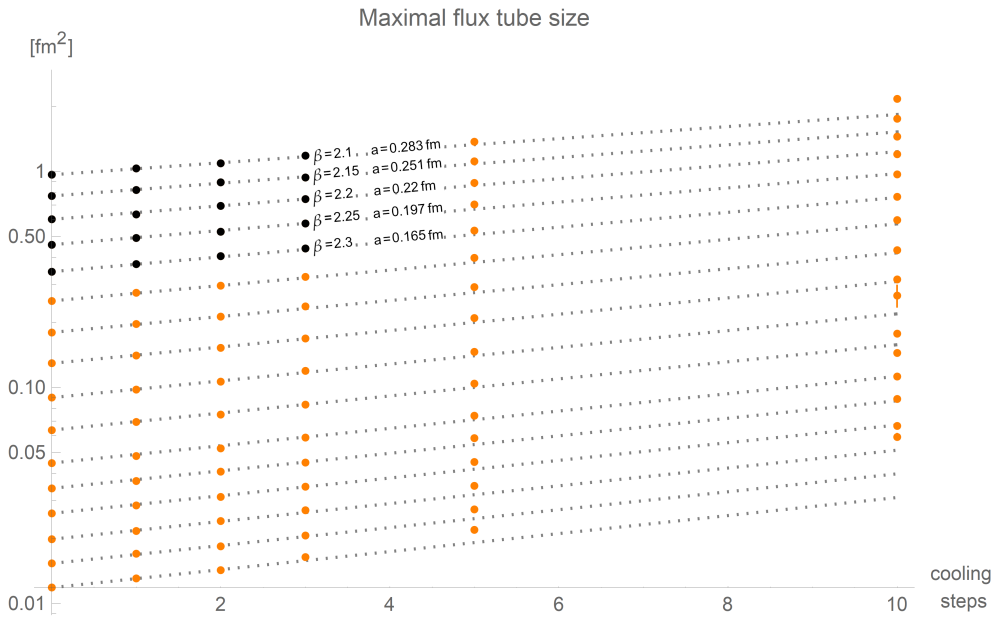

Figure 9. The measured data of the maximal flux tube cross-section for various numbers of cooling steps and several β are shown by black and orange points. The dashed lines depict the fits according to Equation (7), where only the black data points were used. The corresponding fit parameters are given in Table 3. Deviations of the data from the fits can be related to finite size effects.

maximal cross-sections	Estimate	t-Statistic	P-Value
g_{cool}	0.0999(10)	9.1369	$3.5 * 10^{-8}$
g_{discret}	-0.13(5) fm^{-1}	-2.61939	$1.7 * 10^{-2}$

Table 3: Shown are the parameters of the model described by Equation (7) and depicted in Figure 9 for maximal cross-sections.

the P-plaquettes belong to correlated piercings and can be attributed to short range fluctuations. We define the quantity A_{max} as the non-overlapping area around vortex centers.

The vortex density ϱ_{vort} is usually calculated by dividing the number P-plaquettes by the total plaquette number. Given enough statistics it can be determined by counting the number of piercings N_{vort} within a sufficiently large Wilson loop of Area A_{loop} build by N_{loop} plaquettes

$$\varrho_{\text{vort}} = \frac{N_{\text{vort}}}{N_{\text{loop}}} = \frac{N_{\text{vort}}}{A_{\text{loop}} * a^{-2}} = \frac{N_{\text{vort}}}{(A_{\text{free}} + N_{\text{vort}} * A_{\text{max}}) * a^{-2}}. \tag{8}$$

In the last identity we have split the area of the loop into two non-overlapping parts: each piercing is enclosed by circular area given by A_{max} and A_{free} covers the remaining part of the loop. When cooling is applied we have to take into account that A_{max} grows.

$$\varrho_{\text{vort}}(N_{\text{cool}}) = \frac{N_{\text{vort}}}{(A_{\text{free}} + N_{\text{vort}} * (A_{\text{max}}(0) + \delta A_{\text{max}}(N_{\text{cool}}))) * a^{-2}}. \tag{9}$$

Preprints (www.preprints.org) | NOT PEER-REVIEWED | Posted: 25 March 2021 doi:10.20944/preprints202103.0615.v1

Using $A_{\text{loop}} = A_{\text{free}} + N_{\text{vort}} * A_{\max}(0)$ and a model of the form given in Eq. (7) for $A_{\max}(N_{\text{cool}})$ we attain $\delta A_{\max} = A_{\max}(0)(e^{N_{\text{cool}}\ (g_{\text{cool}}+g_{\text{discrete}}\ a)} - 1)$. It follows

$$\varrho_{\text{vort}}(N_{\text{cool}}) = \frac{\varrho_{\text{vort}}(0)}{1 + \varrho_{\text{vort}}(0)\ A_{\max}(0) a^{-2}\ (e^{N_{\text{cool}}\ (g_{\text{cool}}+g_{\text{discrete}}\ a)} - 1)}. \tag{10}$$

We fit g_{cool}, g_{discrete} and $A_{\max}(0)$ to the measurements of ϱ_{vort}. The measured data and the fit are shown in Figure 10. The respective fit parameters are listed in Table 4. The

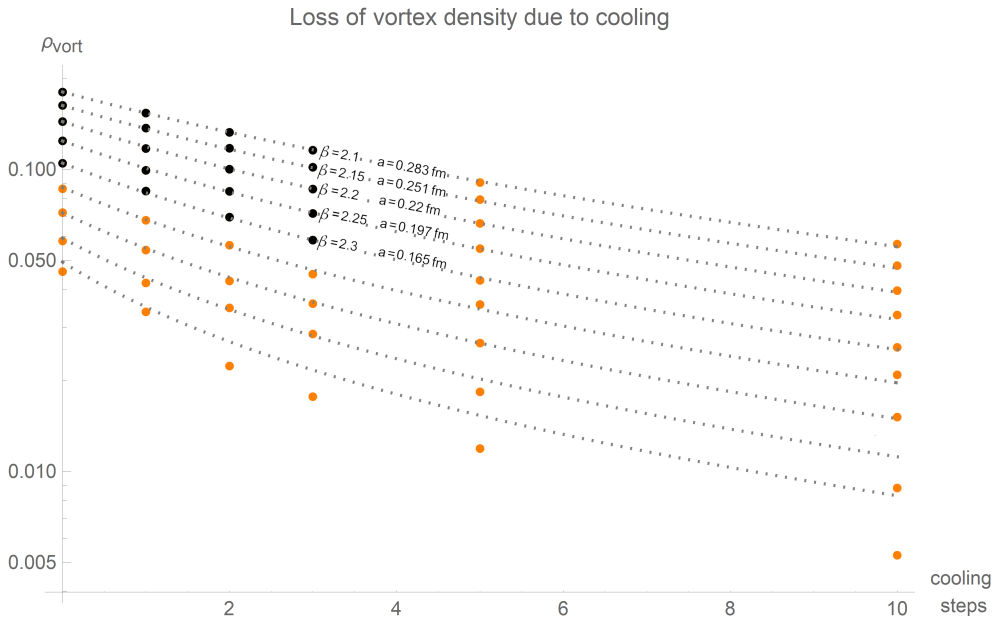

Figure 10. Depicted is the vortex density. For the model prediction shown as dashed lines only the black data points were used. That the data points fall below the model prediction at specific numbers of cooling steps for different values of β can be explained by finite size effects. The corresponding parameters of the model are given in Table 4.

vortex density	Estimate	t-Statistic	P-Value
g_{cool}	0.035(1)	26.5368	$2.8 * 10^{-15}$
g_{discret}	0.066(2) fm^{-1}	27.6254 fm^{-1}	$1.5 * 10^{-15}$
$A_{\max}(0)$	1.41(5)fm^2	25.8937 fm^2	$4.2 * 10^{-}15$

Table 4: The parameters of the model described by Equation (10) for the loss of the vortex density during cooling.

value of $A_{\max}(0)$ is larger than the flux tube cross-sections depicted in Figures 8. This and the fact that the value of g_{cool} for the vortex density is smaller than those of the vortex flux tube cross-sections indicate that the majority of piercings stay separated from one another even when cooling is applied. Assuming circular geometry we can calculate the minimal possible distance between vortex centers

$$d_{\text{center}}(N_{\text{cool}}) = 2\sqrt{\frac{A_{\max}(N_{\text{cool}})}{\pi}}. \tag{11}$$

The minimal available separation s_{flux} of neighbouring piercings can be estimated by

$$s_{\text{flux}}(N_{\text{cool}}) = \underbrace{2\sqrt{\frac{A_{\max}(0)}{\pi}}}_{d_{\text{center}}(0)} - \underbrace{2\sqrt{\frac{A_{\text{vort}}(N_{\text{cool}})}{\pi}}}_{d_{\text{flux}}(N_{\text{cool}})}. \tag{12}$$

Preprints (www.preprints.org) | NOT PEER-REVIEWED | Posted: 25 March 2021 doi:10.20944/preprints202103.0615.v1

If this separation becomes smaller than one lattice spacing our methods of center vortex detection will likely fail: we can no longer find two non-overlapping non-trivial center regions enclosing the thick vortex flux tubes. From this we derive two relevant limits for the lattice spacing a and the lattice extent L

$$a < s_{\text{flux}} \quad \text{and} \quad L > \text{Max}(2\overline{d_{\text{flux}}}, \text{Max}(d_{\text{flux}})). \tag{13}$$

The requirement for the lattice extent L is based on the fact, that two vortex piercings have to fit in every two dimensional slicing through the lattice. Assuming a vanishing minimal flux tube size, the limit is given either by two times the average diameter $\overline{d_{\text{flux}}}$ or one times the maximal diameter $\text{Max}(d_{\text{flux}})$ - whatever is bigger.

Using what we learned so far, we can evaluate these inequalities and find numerical values for the upper limit of a and the lower limit of L. These are depicted in Figure 11 and will now be discussed. Discretization effects are neglected by setting $g_{\text{discret}} = 0$. Fitting the average flux tube cross-sections for configurations without cooling, see Figure 8, by a polynom up to quadratic order with respect to the lattice spacing a gives

$$\overline{A_{\text{vort}}}(0) \approx 3.36691\ a^2 + 0.200467\ \text{fm}\ a, \tag{14}$$

compatible to the values we found in [21]. A fit to the maximal cross-sections without cooling, see Figure 9, results in higher fit parameters

$$Max(A_{\text{vort}}(0)) \approx 11.3\ a^2 + 0.223\ \text{fm}\ a. \tag{15}$$

Using this fit and Eq. (12) with $A_{\text{max}}(0)$ from Table 4 we obtain an upper limit for the lattice spacing that depends on the number of cooling steps and g_{cool}. With this limit we can determine a lower limit for the required lattice extent. Both limits are shown in Figure 11 for the two different values of g_{cool} resulting from average and maximal flux tube sizes from Tables 2 and 3. Let us remember how these limits have been derived: Closed flux lines require that there is sufficient room for two piercings within each two dimensional slice through the lattice - a lower limit for the lattice extent arises.

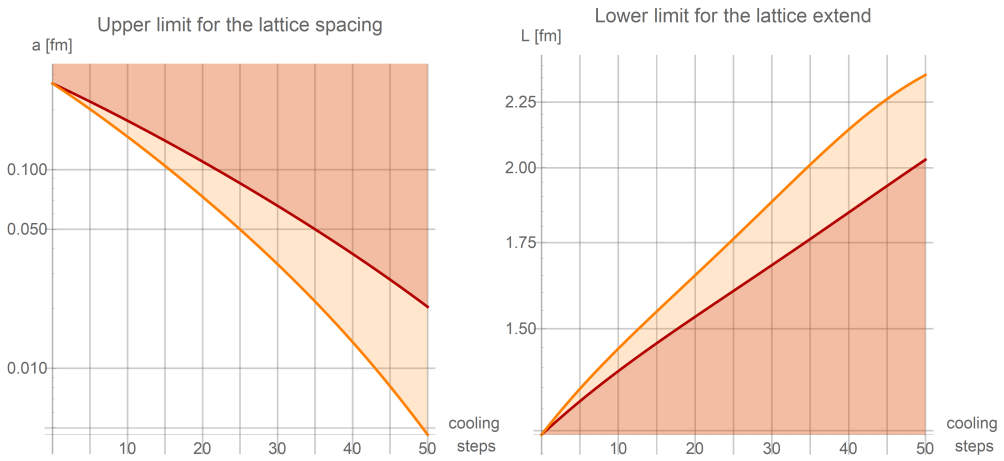

Figure 11. Based on the growth of the flux tubes and the reduction of the vortex density in dependency of the number of cooling steps an upper limit for the lattice spacing (left) and a lower limit for the lattice extent (right) can be derived, as given in Equation (13). The weaker limit depicted in red is based on the slower growth of the maximal sized flux tubes with $g_{\text{cool}} = 0.0999$ (see Table 3), the stronger limit, depicted in orange, is based on the faster growth of average sized flux tubes with $g_{\text{cool}} = 0.14$ (see Table 2).

Taking the stronger limits with $g_{\text{cool}} = 0.14$ we determine corresponding limits of β for given lattice size and number of cooling steps. In Table 5 some numerical values

Preprints (www.preprints.org) | NOT PEER-REVIEWED | Posted: 25 March 2021 doi:10.20944/preprints202103.0615.v1

are shown. We now take a look at the meaning of these limits for the string tension.

$N_{\text{cool}} \setminus L$	8	10	14	20	30	40	50
0	2.12 2.32	2.12 2.39	2.12 2.48	2.12 2.58	2.12 2.73	2.12 2.84	2.12 2.92
1	2.14 2.31	2.14 2.38	2.14 2.48	2.14 2.58	2.14 2.73	2.14 2.83	2.14 2.91
2	2.16 2.31	2.16 2.38	2.16 2.47	2.16 2.58	2.16 2.72	2.16 2.83	2.16 2.91
3	2.19 2.3	2.19 2.37	2.19 2.47	2.19 2.57	2.19 2.71	2.19 2.82	2.19 2.9
5	2.23 2.29	2.23 2.36	2.23 2.46	2.23 2.56	2.23 2.7	2.23 2.81	2.23 2.89
10	None	2.34 2.34	2.34 2.44	2.34 2.54	2.34 2.67	2.34 2.78	2.34 2.86
15	None	None	None	2.44 2.52	2.44 2.65	2.44 2.76	2.44 2.84
20	None	None	None	None	2.54 2.63	2.54 2.73	2.54 2.82
25	None	None	None	None	None	2.66 2.71	2.66 2.79

Table 5: For different numbers of cooling steps and different lattice extents the table gives a lower and an upper limit for β. "None" indicates that the limits exclude one another.

In Figure 4 we observe that the deviation from the asymptotic prediction decreases with increasing β in the low β-regime. We believe that this behaviour holds within the β-intervals of Table 5. The upper limit of β can be extended by increasing the lattice size. It would be interesting to see, if this alone suffices to restore full compatibility with the asymptotic string tension with modest cooling, but the required computational power might exceed the capabilities of our times.

4. Discussion

Using non-trivial center regions we analyzed how Pisa-cooling influences the cross-sections of thick center vortices. We found an exponential growth that slows down with increasing cross-sections. By geometric arguments we derived an upper limit for the lattice spacing above which discretization effects trouble the vortex detection and a lower limit for the lattice extent where finite size effects set in. This window gets smaller with cooling and decreasing lattice extent. Cooling results in deviations from the asymptotic behaviour: an underestimation of the string tension occurs. Within the window increasing β leads to better agreement with the asymptotic behaviour. It would be interesting to see whether the string tension calculated on the projected lattice is in fact fully restored with sufficiently large β or if only a partial restoration occurs.

By improving the method of center vortex detection it might be possible to soften the aforementioned limits. The method of vortex detection used in this work was based on the direct maximal center gauge guided by non-trivial center regions [15–17]: we identify regions whose perimeter evaluates to the non-trivial center element and preserve their evaluation during gauge fixing and center projection. This approach comes with three possibilities of improvement:

The growth of the flux tube due to cooling results in the non-trivial center factors within the evaluation of Wilson loops being spread over more and more links. The original direct maximal center gauge minimizes a gauge functional which takes only those eight links into account that are connected to the respective lattice point. By taking also those links into account that are connected to neighbouring lattice points the troubles arising from the spread of the center flux could be counteracted.

When two thick vortices are not separated by at least one lattice spacing the identification of non-trivial center regions enclosing the single piercings might fail. The original method used for the detection of non-trivial center regions is based on enlarging the perimeter of Wilson loops while preventing overlaps of the resulting regions: if overlaps occurred, the region that evaluates to a higher trace gets deleted. By allowing overlaps an improvement might be possible: more non-trivial center regions are kept to guide the further gauge fixing procedure.

With rising number of cooling steps more non-trivial center regions than P-plaquettes were found: The direct maximal center gauge failed to preserve some of the non-trivial center regions. This could be counteracted by inserting non-trivial factors before starting the simulated annealing procedure which is used to maximize the gauge functional. These non-trivial factors should guaranty that each non-trivial center region evaluates to the non-trivial center element when evaluated in the center projected configuration.

Author Contributions: Conceptualization, R.G.; methodology, R.G.; software, R.G. and M.F.; writing—original draft preparation, R.G.; writing—review and editing, R.G. and M.F.; supervision, M.F.; project administration, M.F.; All authors have read and agreed to the published version of the manuscript.

Funding: This research received no external funding

Institutional Review Board Statement: Not applicable

Informed Consent Statement: Not applicable

Data Availability Statement: The data presented in this study are available on request from the corresponding author.

Acknowledgments: We thank the company *Huemer-Group* (www.huemer-group.com, accessed on 3rd March 2021) and Dominik Theuerkauf for providing the computational resources speeding up our calculations.

Conflicts of Interest: The authors declare no conflict of interest.

References

1. 't Hooft, G. On the phase transition towards permanent quark confinement. *Nuclear Physics B* **1978**, *138*, 1 – 25. doi:https://doi.org/10.1016/0550-3213(78)90153-0.
2. Cornwall, J.M. Quark confinement and vortices in massive gauge-invariant QCD. *Nuclear Physics B* **1979**, *157*, 392 – 412. doi:https://doi.org/10.1016/0550-3213(79)90111-1.
3. Del Debbio, L.; Faber, M.; Giedt, J.; Greensite, J.; Olejnik, S. Detection of center vortices in the lattice Yang-Mills vacuum. *Phys. Rev.* **1998**, *D58*, 094501, [arXiv:hep-lat/hep-lat/9801027]. doi:10.1103/PhysRevD.58.094501.
4. Faber, M.; Höllwieser, R. Chiral symmetry breaking on the lattice. *Prog. Part. Nucl. Phys.* **2017**, *97*, 312–355. doi:10.1016/j.ppnp.2017.08.001.
5. Höllwieser, R.; Schweigler, T.; Faber, M.; Heller, U.M. Center Vortices and Chiral Symmetry Breaking in SU(2) Lattice Gauge Theory. *Phys. Rev.* **2013**, *D88*, 114505, [arXiv:hep-lat/1304.1277]. doi:10.1103/PhysRevD.88.114505.
6. Höllwieser, R.; Schweigler, T.; Faber, M.; Heller, U.M. Center vortices and topological charge. *PoS* **2012**, *ConfinementX*, 078. doi:10.22323/1.171.0078.
7. Golubich, R.; Golubich, R.; Faber, M. Properties of SU(2) Center Vortex Structure in Smooth Configurations. *Particles* **2021**. doi:10.3390/particles4010011.
8. Kovacs, T.G.; Tomboulis, E.T. On P vortices and the Gribov problem. *Phys. Lett. B* **1999**, *463*, 104–108, [hep-lat/9905029]. doi:10.1016/S0370-2693(99)00944-2.
9. Bali, G.S.; Schlichter, C.; Schilling, K. Observing long color flux tubes in SU(2) lattice gauge theory. *Physical Review D* **1995**, *51*, 5165–5198. doi:10.1103/physrevd.51.5165.
10. Booth, S.P.; Hulsebos, A.; Irving, A.C.; McKerrell, A.; Michael, C.; Spencer, P.S.; Stephenson, P.W. SU(2) potentials from large lattices. *Nucl. Phys.* **1993**, *B394*, 509–526, [arXiv:hep-lat/hep-lat/9209007]. doi:10.1016/0550-3213(93)90023-I.
11. Michael, C.; Teper, M. Towards the Continuum Limit of SU(2) Lattice Gauge Theory. *Phys. Lett.* **1987**, *B199*, 95–100. doi:10.1016/0370-2693(87)91469-9.
12. Perantonis, S.; Huntley, A.; Michael, C. Static Potentials From Pure SU(2) Lattice Gauge Theory. *Nucl. Phys.* **1989**, *B326*, 544–556. doi:10.1016/0550-3213(89)90141-7.

13. Bali, G.S.; Fingberg, J.; Heller, U.M.; Karsch, F.; Schilling, K. The Spatial string tension in the deconfined phase of the (3+1)-dimensional SU(2) gauge theory. *Phys. Rev. Lett.* **1993**, *71*, 3059–3062, [arXiv:hep-lat/hep-lat/9306024]. doi:10.1103/PhysRevLett.71.3059.
14. Campostrini, M.; Di Giacomo, A.; Maggiore, M.; Panagopoulos, H.; Vicari, E. Cooling and the String Tension in Lattice Gauge Theories. *Phys. Lett. B* **1989**, *225*, 403–406. doi:10.1016/0370-2693(89)90590-X.
15. Golubich, R.; Faber, M. The Road to Solving the Gribov Problem of the Center Vortex Model in Quantum Chromodynamics. *Acta Physica Polonica B Proceedings Supplement* **2020**, *13*, 59–65. doi:10.5506/APhysPolBSupp.13.59.
16. Golubich, R.; Faber, M. Center Regions as a Solution to the Gribov Problem of the Center Vortex Model. *Acta Physica Polonica B Proceedings Supplement* **2021**, *14*, 87. doi:10.5506/aphyspolbsupp.14.87.
17. Golubich, R.; Faber, M. Improving Center Vortex Detection by Usage of Center Regions as Guidance for the Direct Maximal Center Gauge. *Particles* **2019**. doi:10.3390/particles2040030.
18. Bornyakov, V.G.; Komarov, D.A.; Polikarpov, M.I.; Veselov, A.I. P vortices, nexuses and effects of Gribov copies in the center gauges. Quantum chromodynamics and color confinement. Proceedings, International Symposium, Confinement 2000, Osaka, Japan, March 7-10, 2000, 2002, pp. 133–140, [arXiv:hep-lat/hep-lat/0210047].
19. Kovacs, T.G.; Tomboulis, E.T. Vortex structure of the vacuum and confinement. *Nucl. Phys. B Proc. Suppl.* **2001**, *94*, 518–521, [hep-lat/0010076]. doi:10.1016/S0920-5632(01)00899-4.
20. Kovács, T.G.; Tomboulis, E. Bound on the string tension by the excitation probability for a vortex. *Nuclear Physics B - Proceedings Supplements* **2000**, *83-84*, 553–555. doi:10.1016/s0920-5632(00)91736-5.
21. Golubich, R.; Faber, M. Thickness and Color Structure of Center Vortices in Gluonic SU(2) QCD. *Particles* **2020**, *3*, 444–455. doi:10.3390/particles3020031.